Original Research

Study on Water Diffusion Characteristics in the *In-situ* Soil of Exfiltration Type Bioretention

Junkui Pan[1]*, Ruiqiang Ni[2], Yongcun Zhang[1], Jinxin Li[3]

[1]School of Civil and Transportation Engineering, Henan University of Urban Construction, Longxiang Avenue, Xinhua District, Pingdingshan 467000, China
[2]China Railway 10th Bureau Group Investment Development Co., Ltd, China Railway Caizhi Industrial South Road, Lixia District, Jinan 250001, China
[3]Highway School, Chang'an University, South 2nd Ring Road, Xian, 710064, China

Abstract

Exfiltration type bioretention can collect rainwater runoff to recharge groundwater, but the water diffusion in the *in-situ* soil can have an impact on the foundation of adjacent structures (such as roads). Generally, the existing studies are primarily focused on the exfiltration of bioretention as an index of runoff control or the water balance. However, research is lacking on the diffusion characteristics of soil water content in different *in-situ* soils. Therefore, in this study, the VADOSE/W model was used to simulate the water transport process of bioretention ponds and *in-situ* soils, under long-term rainfall. The water diffusion characteristics of four *in-situ* soils were studied: silt loam (SL), loam (L), sandy clay loam (SCL), and sandy loam (SaL). The results showed that under 12 rainfall events, with a monthly maximum rainfall of 268 mm in the study area, for four *in-situ* soil types, the bioretention pond's bottom exfiltration volume per unit area reached 3.93–7.91 times that of the lateral. The order of bottom exfiltration volume was SaL>SCL>L>SL. Over time, the *in-situ* soil water content fluctuated with rainfall events. The order water content was usually SL>L>SCL>SaL, and the water diffused into the *in-situ* soil was distributed in a symmetrical arc along the horizontal direction. After rainfall events, at depths of 1, 3 and 5 m, for SL, L, SCL, and SaL soils, the lateral water diffusion ranges were ~1.25-1.47 m, ~1.23-1.45 m, ~1.22-1.77 m, and ~1.46-1.60 m, respectively. With a continuous supply of water, the horizontal diffusion distance of each *in-situ* soil tended to be the same, although the water diffusion range of SCL was relatively larger. Therefore, when an exfiltration type bioretention area is designed, the distance between the bioretention edge and the adjacent structures should be

*e-mail: 15303950218@163.com

more than 2 m to avoid nearby structural foundations being negatively affected by water seepage over a long period of time.

Introduction

With the acceleration of global urbanization, permeable natural land cover (such as natural forest and grassland), and other land use (such as farmland) has been increasingly replaced by buildings and roads [1]. The impermeable areas of urban areas have increased sharply, causing a series of serious risks and impacts on the urban water environment [2]. First, during a rainfall event, infiltration decreases significantly, while the surface runoff increases accordingly, which can result in frequent urban floods [3]. Second, the groundwater in urban areas cannot be effectively recharged, causing a drop in its level, which can result in land subsidence [4-5]. Additionally, urban surface runoff usually contains pollutants, such as nutrients and salts, heavy metals, suspended solids, hydrocarbons, and pathogens, which flow into the downstream water system through the urban drainage system. Consequently, the regional water resources become polluted, and also threaten human health [6-10].

With the continuous deterioration of global water resources, low-impact development (LID) concepts have been proposed. During regional development, ecological landscapes, such as permeable pavements, green roofs, grassed swales, bioretention ponds (or areas), man-made wetlands, and stabilization ponds [11-13], are used to control and utilize rainwater runoff from the source, to achieve local decentralized management of rainwater [14-16]. Among them, bioretention has become a promising and practical ecological control measure for rainwater management, owing to the integration of functions, such as landscape, runoff control, and water purification [17-19]. A typical cross-section of a bioretention pond is shown in Fig. 1. The design scale of a bioretention pond is generally 5-10% of its catchment area. The design usually consists of 150-300 mm aquifer, 50-80 mm mulch, 300-700 mm plant soil layer, and 150-300 mm sand-gravel drainage layer [20-22]. When the soil permeability is lower than 1.27 cm/h, or the bioretention structure is an anti-seepage (impermeable) type, an underdrain with a diameter of 50-100 mm is buried in the sand-gravel layer to enhance drainage [23-24]. During rainfall events, when the rainwater runoff flows through the bioretention pond, the filler layer will temporarily intercept and store the runoff. Some runoff will slowly seep into the surrounding soil, which will recharge the groundwater, and some will diffuse into the atmosphere through evaporation and transpiration, which simulates the natural hydrological conditions, prior to regional development [25-26].

Recently, there have been studies of the runoff regulation effect of bioretention ponds through laboratory and field experiments. For example, Winston [27], Pan [28], and Gülbaz [29] have proved that bioretention can effectively reduce the runoff volume and attenuates the peak runoff. Debusk [30] found that bioretention outflow can simulate the process of shallow water discharge into rivers in undeveloped areas, thereby helping to restore the natural regional hydrological cycle. To alleviate the continuous decline of groundwater levels, research has been carried out on the recharge effect of bioretention ponds on groundwater. For example, through field experiments Guo [31] showed that the concentrated infiltration of runoff by bioretention had a significant effect on groundwater recharge. Pan [32] studied the long-
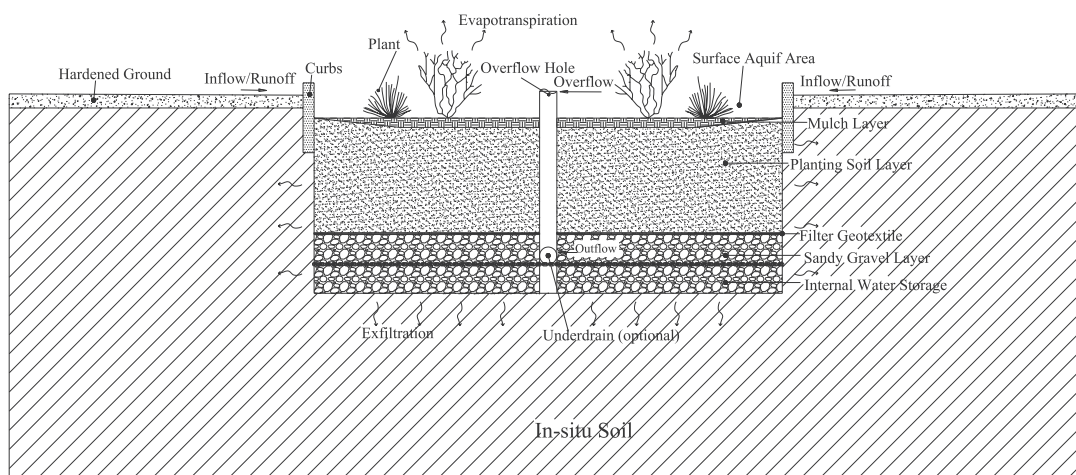

Fig. 1. Diagram of a typical bioretention pond.

term water balance of bioretention areas and showed that the amount of water exfiltrating the ground from bioretention accounted for the largest proportion (more than 50% of the total runoff volume). Gao [33] showed that the type of *in-situ* soil is the main factor affecting exfiltration from the bioretention area.

A bioretention pond is typically used to collect rainwater runoff from pavements or building roofs and is located close to the structures. When a bioretention pond is used for the concentrated infiltration of rainwater, it typically needs to collect runoff of 5-20 times its own area, causing a large amount of rainwater to seep underground [34]. If the water continues to spread to the adjacent structure foundation, the safety of the structure will be affected. For example, Liang [35] showed that a large amount of bioretention water diffused to the road subgrade, resulting in a significant settlement of the pavement. Presently, the commonly used method is to carry out anti-seepage treatment for bioretention; however, this method limits the recharge of rainfall to groundwater [36-37]. Additionally, there are some differences in the properties for underground soil in different regions, resulting in different water diffusion characteristics. Therefore, the study on the diffusion characteristics of water from bioretention areas in *in-situ* soil can provide a basis for the layout and design of a bioretention pond.

Owing to the lack of direct observations of water diffusion in soil, numerical simulation can provide insight for this study. Currently, few models can be used to simulate the hydrological effects of bioretention, such as RECARGA, HYDRUS-1D, Stormwater Management Model (SWMM), and SUSTAIN. Among them, RECARGA predominantly uses the Green-Ampt equation to simulate the rainwater infiltration process, which is suitable for long-term water balance analyses of bioretention; however, it is unsuitable for simulating the situation of water diffusion in soil [38]. The HYDRUS-1D model is a one-dimensional model based on the Richards equation. However, it disregards the lateral diffusion of soil water, and therefore cannot simulate the lateral water transport process in the soil [39]. The SWMM and SUSTAIN models are based on the LID concept to simulate the runoff process of the whole region, carry out LID planning, and simplify the water transport process within a bioretention area. Therefore, there are clear deficiencies in the study of bioretention alone [40-41]. The VADOSE/W model is a two-dimensional numerical model used for the simulation of soil seepage, groundwater changes, evaporation and evapotranspiration under saturated-unsaturated soil states. It couples the Richards equation and atmospheric boundary conditions to calculate soil water movement and the surface ponding process [42]. Gao [43] used the VADOSE/W model to study the ponding and outflow processes of a bioretention pond collecting runoff from roads and proved that the model can effectively simulate the hydrological effects of two-dimensional bioretention. Additionally, Pan [32] studied the long-term water balance of a two-dimensional bioretention area of an expressway service area, based on the VADOSE/W model.

Presently, most existing studies are focused on the exfiltration of bioretention as an index of runoff control or the water balance. However, studies on the diffusion characteristics of water in different *in-situ* soils are lacking. The research objective of this study was to use the VADOSE/W model to simulate the saturated-unsaturated transport process of rainwater runoff in the bioretention area's soil, and to study the water diffusion characteristics, including (but not limited to) water exfiltration, water content change, and water horizontal diffusion, in different *in-situ* soils under long-term rainfall events. This study can therefore provide a reference for the layout and design of bioretention ponds in different regions.

Experimental Procedures

Soil Saturated-Unsaturated Seepage Control Equation

The top of the bioretention and the soil areas are in direct contact with the air, and the lowest point is a certain distance from the groundwater, and is in a dry-wet cycle, which is the typical saturated-unsaturated soil. The movement of rainwater entering the bioretention and soil includes downward infiltration and lateral diffusion, which can be regarded as horizontal and vertical seepage. Therefore, the two-dimensional Richards seepage equation can be used to describe the water movement process of bioretention and the associated soil [44], as shown in Equation (1):

$$\frac{\partial \theta}{\partial t} = \frac{\partial}{\partial x}\left[k(\theta)\frac{\partial h}{\partial x}\right] + \frac{\partial}{\partial z}\left[k(\theta)\frac{\partial h}{\partial z}\right] + \frac{\partial k(\theta)}{\partial z} - S(x,z,t) \quad (1)$$

where h = the negative pressure head of soil (mm); $k(\theta)$ = the soil permeability coefficient (mm/h); θ = the soil volume water content (mm^3/mm^3); $S(x, z, t)$ = the source sink term, (such as transpiration and evaporation (mm)), and t = the time (h).

When the soil negative pressure head h is ≥ 0, the soil is in a saturated state, and θ and $k(\theta)$ are both fixed values in equation (1), which are the soil saturated water content and the soil saturated permeability coefficient, respectively. When h is <0, the soil is in an unsaturated state. At this time, θ and $K(\theta)$ are variable values, which can be defined according to the Van Genuchten equations [45], which include the soil moisture characteristic curve equation (2) and hydraulic conductivity curve Equation (3):

$$\theta(h) = \begin{cases} \theta_r + \dfrac{\theta_s - \theta_r}{\left[1 + |ah|^n\right]^m} & (h < 0) \\ \theta_s & (h \geq 0) \end{cases} \quad (2)$$

$$K(\theta) = \begin{cases} K_s S_e^{1/2} \left[1 - \left(1 - S_e^{1/m} \right)^m \right]^2 & (h < 0) \\ K_s & (h \geq 0) \end{cases} \quad (3)$$

where θ_r = the soil residual water content (mm³/mm³); θ_s = the soil saturated water content (mm³/mm³); a, n, and m are the Van Genuchten parameters, and $m = 1 - 1/n$; S_e = the effective saturation, $S_e = (\theta - \theta_r)/(\theta_s - \theta_r)$, and K_s = the soil saturated permeability coefficient (mm/h).

Design Rainfall

When studying the effects of bioretention on the hydrological cycle of the area, the design rainfall should first be determined. It takes a certain length of time for water diffusion in the soil around the bioretention pond; therefore, to reflect the impact of the lag on water diffusion, this study used the long-term rainfall data measured in the study area was used as data for the design rainfall. Fig. 2 shows the monthly rainfall data of the study area in 2010. The total annual rainfall was 1,045 mm, which is close to the average annual rainfall (1090 mm) from 1951 to 2013 in the study area; the maximum was 268 mm in July with 12 rainfall events, accounting for 25.63% of the annual total. The hourly rainfall data in July 2010 was selected
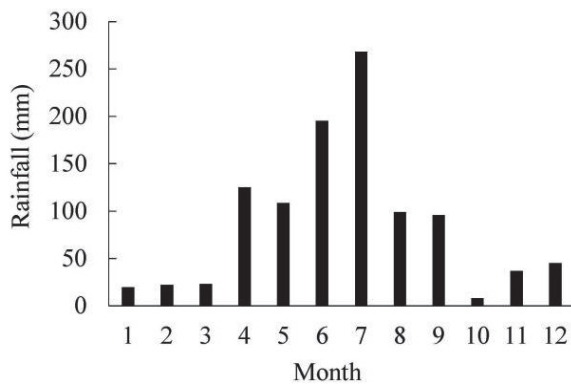

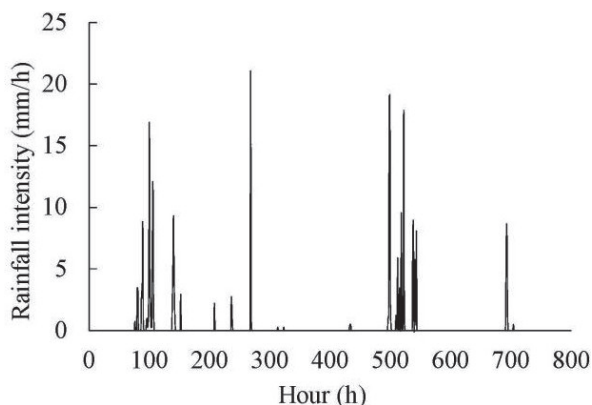Fig. 2. Monthly rainfall data in the study area for 2010.

Fig. 3. Hourly rainfall data of the study area in July 2010.

to use as the rainfall intensity for the calculation of the design intensity, as shown in Fig. 3.

The runoff entering the bioretention pond is composed of the catchment runoff and direct rainfall into the pond [43]. The design runoff intensity was calculated using Equation (4):

$$q_0 = \frac{q(\psi F_0 + F_1)}{F_1} \quad (4)$$

where q_0 = the design runoff intensity acting on bioretention (mm/h); q = the actual rainfall intensity (mm/h); Ψ = the runoff coefficient (which was 0.9 in this study); F_0 = the catchment area (m²); and F_1 = the bioretention area (m²).

Design Parameters

Bioretention Design Parameters and In-situ Soil Types

The VADOSE/W model was used to simulate the water transport process within the bioretention pond and four *in-situ* soils; the bioretention design parameters and *in-situ* soil types are shown in Table 1. The four *in-situ* soils include silt loam (SL), loam (L), sandy clay soil (SCL), and sandy loam (SaL). The size of the bioretention area were all taken as 10% of the catchment area, and included layers of planting soil, sandy-gravel and mulch, with thicknesses of 700 mm, 300 mm, and 50 mm, respectively. The depth of surface aquifer was 300 mm. To ensure the maximum infiltration into the soil, the impact of overflow was not considered in the numerical simulation, and the rainwater runoff was allowed to accumulate on the bioretention surface area. Soil types SL and L had permeability coefficients lower than 1.27 cm/h, and an underdrain (diameter of 50 mm) set in the middle of the sandy-gravel layer, to form an internal water storage area at a height of 150 mm. However, for soil types SCL and SaL, these parameters were not set. The evaporation and transpiration volumes are much smaller than the exfiltration volume of the bioretention pond; therefore, these were not considered in this study. Additionally, the influence of the groundwater level was also not considered.

Soil Hydraulic Characteristic Parameters

When the VADOSE/W model is used to simulate the saturated-unsaturated water transport process of the pond and *in-situ* soil, the soil hydraulic characteristic parameters need to be determined, as shown in Table 2. In this study, the hydraulic parameters of the planting soil and sandy-gravel layer used the data which was verified through studies on the influence of bioretention parameters on the regulation effects of road runoff [43], while the parameters of four *in-situ* soil types were taken from Li, who studied the unsaturated seepage process of rainwater infiltration into a ditch [46].

Table 1. Bioretention design parameters and *in-situ* soil type.

Simulated situation	Bioretention design parameters						*In-sit*u soil type
	Area ratio of bioretention to catchment area	Thickness of mulch (mm)	Depth of surface aquifer (mm)	Thickness of planting soil (mm)	Thickness of sandy- gravel layer (mm)	Height of internal water storage (mm)	
SL	10%	50	300	700	300	150	Silt loam
L						150	Loam
SCL						No	Sandy clay loam
SaL						No	Sandy loam

Table 2. Soil hydraulic characteristic parameters of bioretention and *in-situ* soils.

Soil type	Saturated permeability coefficient (cm·h^{-1})	Residual water content (cm^3·cm^{-3})	Saturated water content (cm^3·cm^{-3})	a(cm^{-1})	n	m
Bioretention						
Planting soil	5.04	0.058	0.408	0.057	2.00	0.50
Sandy-gravel	163.00	0.046	0.445	0.153	2.64	0.62
In-situ soil						
Silt loam	0.45	0.067	0.450	0.020	1.41	0.29
Loam	1.04	0.078	0.432	0.036	1.56	0.36
Sandy clay loam	1.31	0.100	0.393	0.059	1.48	0.32
Sandy loam	4.43	0.065	0.416	0.075	1.89	0.47

The initial water content of the bioretention filler and *in-situ* soil is the water content distribution after the free drainage of the medium, reaching stability under the saturated state.

Model Grid and Boundary Condition

In this study, the lateral and vertical dimensions of bioretention were both set at 1 m. To reduce the influence of the boundary effect, the lateral range of the soil on both sides of the pond were taken as five times the width of the pond, and the vertical range extends downward from the bottom of the pond to five times the height of the pond. In this study, a rectangular grid was used to divide the model. In the lateral direction, the bioretention range and the width of 1 m on both sides were properly densified, and the grid size was 10 cm, and the others were set at 20 cm. Vertically, the surface layer of the bioretention area is significantly affected by atmospheric conditions. Therefore, the unique surface function of the VADOSE/W model was used to create a 30 cm upper layer of planting soil as the surface unit. The grid was finely divided, at a height of 3 cm, and the lower 40 cm of the planting soil was set to 5 cm. Owing to the relatively larger permeability coefficient of the sandy-gravel layer, to ensure the convergence of the simulation results, the grid of the sandy-gravel layer was refined. The grid height and the boundary grid size of the underdrain in the sandy-gravel layer were both

set to 3 cm. The grid 1 m below the pond was split into 10 cm intervals, and the others were set to 20 cm. Curbs are typically set on both sides of the pond; therefore, a 30 cm impermeable interface was set above the contact surface between the bioretention pond and soil.

The surface of the pond receives runoff and concentrates the infiltration. When the runoff intensity is greater than the infiltration capacity of the bioretention filler, water will accumulate on the surface. The boundary conditions of atmospheric ponding in the model were used for this process. For bioretention with an underdrain, when the water does not reach the underdrain, the water flow of which is 0, and when the water reaches, the water pressure of which is 0, so the boundary of underdrain can use the seepage surface boundary conditions. The influence of groundwater level was not considered; therefore, free drainage boundary conditions were set at the lowest soil layer. The grid division results and boundary conditions of the bioretention pond and soil are shown in Fig. 4.

Results and Discussion

Water Exfiltration from Bioretention to *In-situ* Soil

Fig. 5 shows the cumulative exfiltration volume per unit area at the bottom of the bioretention pond and the sides, for the four *in-situ* soil types. Owing
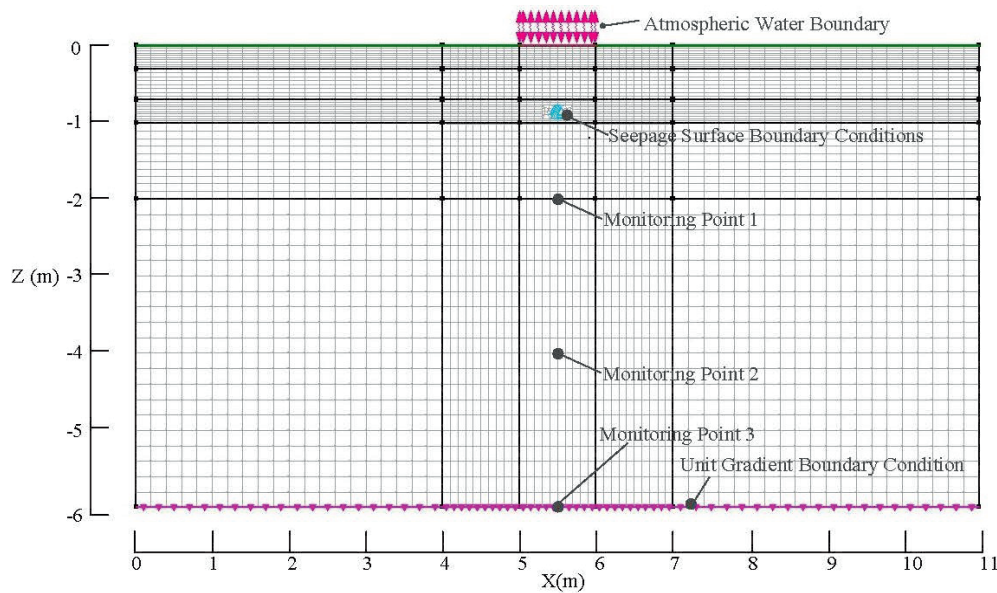
Fig. 4. Simulation model of bioretention pond and *in-situ* soil.

to the difference between the horizontal and vertical structural dimensions of the bioretention area, the use of the exfiltration volume per unit area is more suitable to compare the water diffusion capacities.

Fig. 5 further shows that with the occurrence of rainfall events, the exfiltration from the bottom of the pond increased significantly, while the change trend of lateral exfiltration was relatively flat. This indicates that the exfiltration from the lowest bioretention layer was more sensitive to rainfall. For the four soil types, the cumulative exfiltration volume per unit area at the lateral and bottom of the pond were 196.03-424.99 mm/m² and 1111.84-1981.06 mm/m², respectively. Additionally, the bottom exfiltration volume reached 3.93-7.91 times the lateral exfiltration volume, indicating that the water exfiltration of bioretention was mainly dominated by the bottom.

For the exfiltration from the bottom of the pond, the order of cumulative exfiltration volume for the *in-situ* soil types was SaL>SCL>L>SL, and the volume increased significantly with an increase in the soil saturated permeability coefficient (K_s). Additionally, owing to the smaller K_s of L and SL, the underdrain in the sandy-gravel layer and part of the rainwater was discharged through the underdrain, further reducing the exfiltration volume at the bottom of the pond. The order of the lateral cumulative exfiltration volume for the *in-situ* soil types was SCL>L>SL>SaL. Generally, the impact of soil type on lateral exfiltration was low. However, the lateral exfiltration was relatively larger for SCL. This is predominantly owing to the K_s of SCL, which was much smaller than that of the planting soil. There was no underdrain, so the water accumulated easily at the bottom of the sandy-gravel layer, thereby increasing the lateral exfiltration volume.
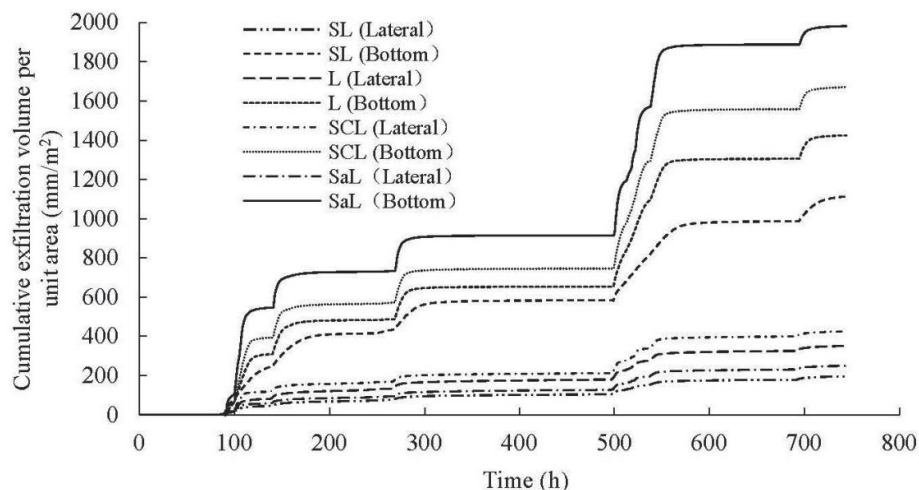

Fig. 5. Cumulative exfiltration volume of bioretention under different *in-situ* soil types.

Water Content Changes in *In-situ* Soil Types

Historical Analysis of Water Content

The water content change processes over the rainfall duration for the four *in-situ* soils under long-term rainfall at monitoring points 1, 2, and 3 (as shown in Fig. 4) are shown in Fig. 6. Monitoring points 1, 2, and 3 correspond to depths directly below the bioretention pond, of 1 m, 3 m, and 5 m, respectively. In the figures, the initial value at 0 h is the water content when the soil drains freely from a saturated to a stable state. At this time, the water content of SL was the largest, and the water content range of monitoring points 1, 2, and 3 was 0.334-0.356. The water content of SaL was the smallest, at 0.109-0.125, while that of L and SCL was between these two, at 0.239-0.263 and 0.232-0.245, respectively. As the depth of the soil increases, the initial water content increases, to a certain extent.

Fig. 6 shows that the *in-situ* soil water content fluctuated with the rainfall events. As the soil depth increased, the influence of rainfall on the soil water content gradually decreased, the lag time of water content change was prolonged, and the degree of fluctuation of the water content was weakened. There were significant differences in the change trend of water content among the *in-situ* soil types, including the effect of rainfall intensity. The water content of SaL and SCL changed more sharply, while that of SL and L was relatively flat. Additionally, the water content of each *in-situ* soil during a rainfall event was different, as follows: SL > L>SCL>SaL. The results show that with
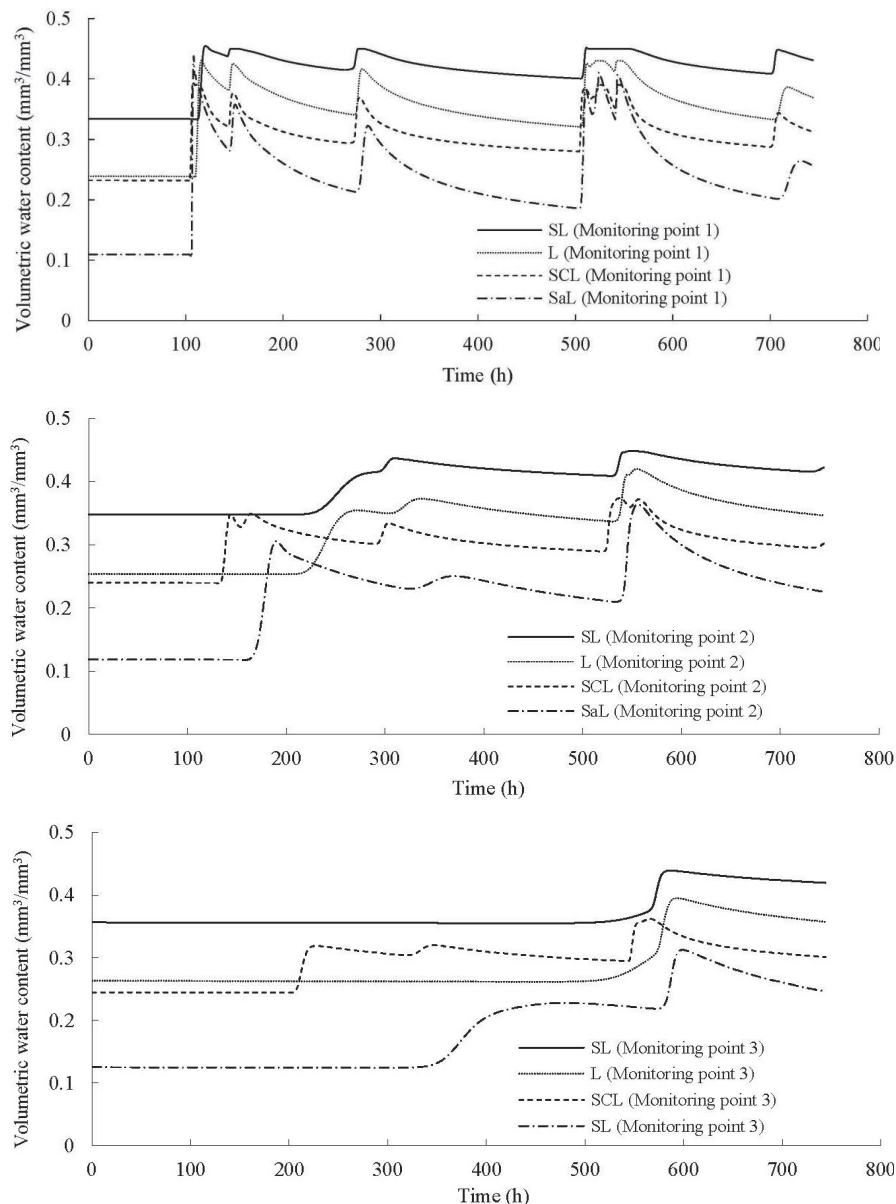

Fig. 6. Water content variation process with rainfall at different monitoring points, for the four *in-situ* soil types: a), b), and c) represent monitoring points 1, 2, and 3, respectively.
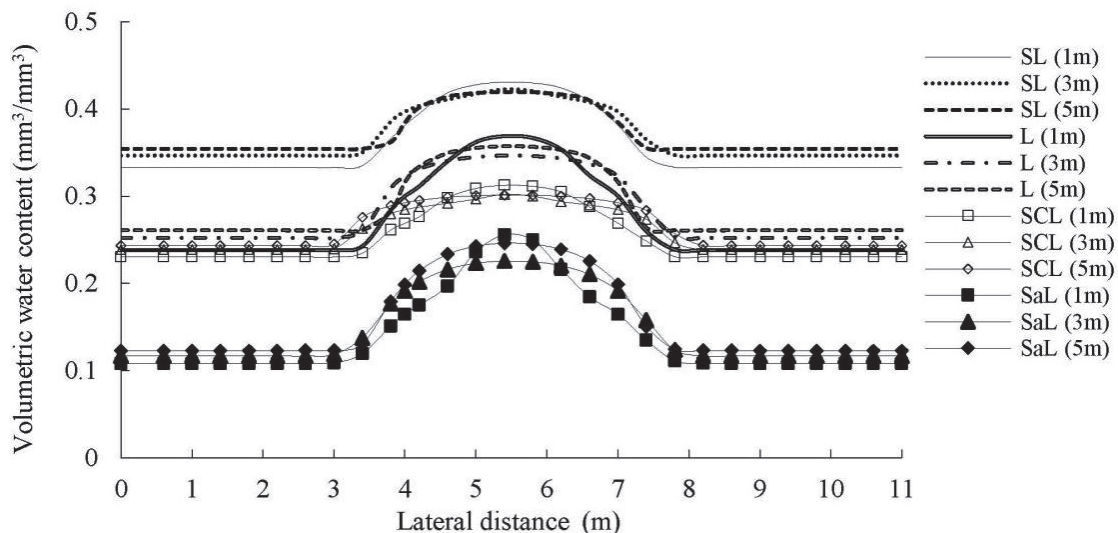
Fig. 7. Water content horizontal distribution of the four *in-situ* soil types, at depths of 1, 3, and 5 m below the bioretention pond.

an increase in soil K_s, the sensitivity of water content to rainfall events was enhanced, and the water content changed more drastically, but its water-holding capacity was weakened. The water in the soil was then easily drained, and the influence on the adjacent structure was relatively smaller.

Additionally, although the K_s of monitoring points 2 and 3 of SaL was larger than that of SCL, the water content change of SaL was prolonged. This was predominantly owing to the lower initial water content of the SaL. This shows a higher volume of pores to be replaced by the water, resulting in less downward diffusion.

Horizontal Distribution of Water Content

The horizontal distribution of water content after rainfall events, at depths of 1, 3, and 5 m below the bioretention pond is shown in Fig. 7, for each *in-situ* soil type. The figure shows that the water content of each soil was different, as follow: SL>L>SCL>SaL. The water content exhibited a symmetrical arc distribution along the horizontal direction, and the water content was highest in the middle of the bioretention area. The water diffused to both sides, creating a gradual decrease in water content until it returned to its initial water content. The soil type had an influence on the horizontal distribution width of the water content. The distribution width of SaL and SCL (~4.5 m) was slightly larger than that of SL and L (~4.0 m). This may be because SL and L soils were equipped with an underdrain, resulting in the reduction of water seepage into the *in-situ* soil. Additionally, when it was close to the bioretention bottom (such as 1 m deep), the water content horizontal distribution of the *in-situ* soil was relatively steeper, which was predominantly due to the fact that the water supply to the soil was greater when near the bioretention.

Historical Analysis of Water Lateral Diffusion of *In-situ* Soil

Fig. 8 shows the lateral water diffusion distance (to the central axis of the bioretention area), at depths of 1, 3, and 5 m below the bioretention pond, for all *in-situ* soils under long-term rainfall. A water lateral diffusion distance of 0 m indicated that the water had not yet reached a certain depth in the *in-situ* soil.

Additionally, when the water collected by the pond has reached a certain depth in the *in-situ* soil, the water initially rapidly diffused laterally. However, as the diffusion distance increased, its rate gradually decreased, and the horizontal range of water tended to gradually stabilize. At depths of 1, 3, and 5 m, the SL, L, SCL, and SaL soils had water diffusion starting times of ~115-533 h, ~12-547 h, ~106-210 h, and ~107-347 h, respectively. With an increase in soil depth, horizontal water diffusion decreased, and the influence of the soil type was enhanced. Compared with SaL and SCL, the K_s of SL and L was relatively smaller, and the underdrain at the bottom of the gravel layer further reduced the amount of exfiltration; thus, the start of their water diffusion was delayed, at the same depth. The K_s of SaL was larger than that of SCL, but its diffusion start time was relatively longer, which was related to the lower initial water content of SaL. When the water diffused downward in SaL, more pore space needed to be filled, resulting in a lower water transport capacity.

The water lateral diffusion ranges for SL, L, SCL, and SaL, were ~1.75-1.97 m, ~1.73-1.95 m, ~1.72-2.27 m, and ~1.96-2.10 m, respectively (after rainfall events, at depths of 1, 3, and 5 m). The results show that the water diffusion range of each *in-situ* soil was different in the early stage (SCL>SaL>L≈SL), and with the continuous supply of water, the water diffusion range of each soil tended to be consistent gradually. At a depth of 1 m
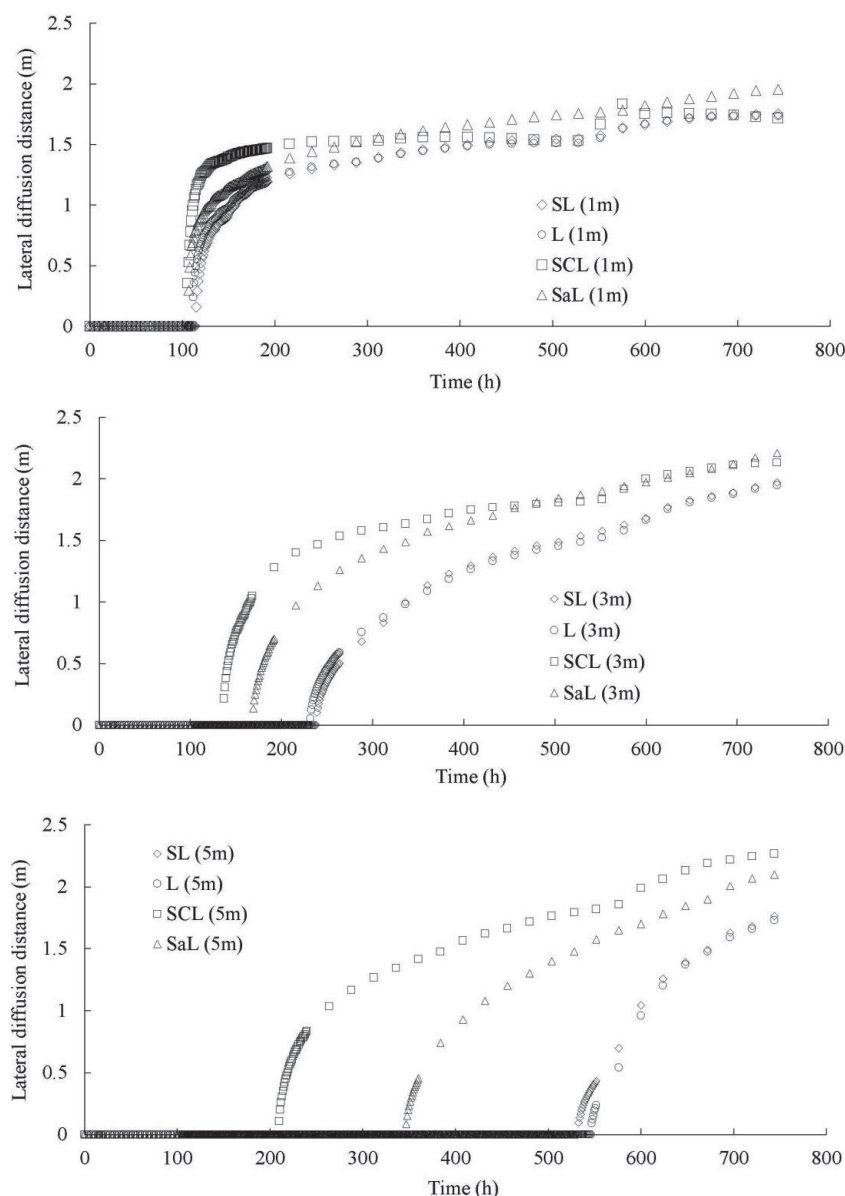
Fig. 8. Water lateral diffusion distance of the four *in-situ* soil types, at varying depths below the bioretention pond: a), b), and c) represent depths of 1, 3, and 5 m, respectively.

below the bioretention pond, there was adequate water supply; therefore, the initial horizontal diffusion rate was higher, and it stabilized earlier than at depths of 3 and 5 m. Additionally, the soil depth had an impact on the water horizontal diffusion range. The maximum water diffusion distance at depths of 1, 3, and 5 m were 1.956 m, 2.208 m, and 2.269 m, respectively, indicating that with the increase in soil depth, the diffusion range also partially increased; however, the increment gradually decreased.

In this study, the design width of the bioretention pond was 1 m; thus, the maximum diffusion distances at depths of 1, 3, and 5 m, were 1.456, 1.708, and 1.769 m, respectively, from the boundary of the pond. Therefore, the maximum water diffusion distance of 2 m, from the edge of the pond, ensured that the

structure foundation was not affected by the exfiltration water of bioretention.

Conclusions

The VADOSE/W model was used to study the water diffusion characteristics of bioretention ponds in different *in-situ* soils, under long-term rainfall. The following conclusions have been made:

The bioretention exfiltration is dominated by seepage from the bottom of the pond, which increases with an increase in *in-situ* soil K_s. When there is a decrease in *in-situ* soil K_s or an increase in depth, the degree of fluctuation of the *in-situ* soil water content response to rainfall is clearly lower. The *in-situ* soil

water content in the center of the bioretention area is the highest, and gradually decreases as water diffuses to the sides. Additionally, with an increase in *in-situ* soil K_s, the *in-situ* soil water content is usually less under rainfall events. With a continuous supply of water, the diffusion range of each *in-situ* soil tended to be consistent. If a bioretention pond does not have an underdrain, when the *in-situ* soil K_s is much smaller than that of the planting soil, the water diffusion rate is usually higher, and the lateral water diffusion range is typically larger.

The results suggest that the *in-situ* soil type has a significant influence on the water diffusion of bioretention and the water content distribution in the *in-situ* soil. However, the *in-situ* soil layering was not considered in this study. It is recommended that further research be conducted on the diffusion characteristics of bioretention water in the layered *in-situ* soil.

Acknowledgments

Conflict of Interest

This manuscript has not been published or presented elsewhere in part or in entirety and is not under consideration by another journal. We have read and understood your journal's policies, and we believe that neither the manuscript nor the study violates any of these. There are no conflicts of interest to declare.

References

1. CHEN Y., LIU T., CHEN R., ZHAO M.K. Influence of the built environment on community flood resilience: evidence from Nanjing city, China. Sustainability, **12** (6), 2401, **2020**.
2. ZHANG J.Y., WANG Y.T., HE R.M., HU Q.F, SONG X.M. Discussion on the urban flood and waterlogging and causes analysis in China. Advances in Water Science, **27** (4), 485, **2016** [In Chinese].
3. CHITWATKULSIRI D., MIYAMOTO H., WEESAKUL S. Development of a simulation model for real-time urban floods warning: a case study at Sukhumvit Area, Bangkok, Thailand. Water, **13** (11), 1458, **2021**.
4. SUNDELL J., ROSEN L., WLADIS D., FRANSSON A., ERICSSON L.O. Assessing the risk of groundwater drawdown induced land-subsidence. IAH International Congress, AQUA2015, Rome, Italy, **2015**.
5. HUANG W.B., YAN C.H., ZHANG X.N., QIU G.Y. The impact of urbanization on groundwater quantity, quality, hydrothermal changes and its countermeasures. Advances in Earth Science, **35** (5), 497, **2020** [In Chinese].
6. ZHANG W., LI J., SUN H.C., CHE W. Pollutant first flush identification and its implications for urban runoff pollution control: a roof and road runoff case study in Beijing, China. Water Science and Technology, **83** (8), 10.2166/wst.2021.157, **2021**.
7. XU J., WU X.D., GE X.G., TIAN Y. Variations of concentration characteristics of rainfall runoff pollutants in typical urban living areas. Bulletin of Environmental Contamination and Toxicology, **106** (4), 608, **2021**.
8. ALMASI A., MAHMOUDI M., MOHAMMADI M., DARGAHI A., BIGLARI H. Optimizing biological treatment of petroleum industry wastewater in a facultative stabilization pond for simultaneous removal of carbon and phenol. Toxin Reviews, **40** (7), 1, **2019**.
9. AZIZI A., DARGAHI A., ALMASI A. Biological removal of diazinon in a moving bed biofilm reactor-process optimization with central composite design.Toxin Reviews, 10.1080/15569543.2019.1675708, **2019**.
10. ALMASI A., DARGAHI A., AMRANE A., FAZLZADEH M., SOLTANIAN M., HASHEMIAN A. Effect of molasses addition as biodegradable material on phenol removal under anaerobic conditions. Environmental Engineering and Management Journal, **17** (6), 1475, **2018**.
11. SHARAFI K., PIRSAHEB M., KHOSRAVI T., DARGAHI A., MORADI M., SAVADPOUR M.T. Fluctuation of organic substances, solids, protozoan cysts, and parasite egg at different units of a wastewater integrated stabilization pond (full scale treatment plant): a case study, Iran. Desalination & Water Treatment, **57** (11), 4913, **2016**.
12. DARGAHI A., MOHAMMADI M., AMIRIAN F., KARAMI A., ALMASI A. Phenol removal from oil refinery wastewater using anaerobic stabilization pond modeling and process optimization using response surface methodology (RSM). Desalination and water treatment, **87** (8), 199, **2017**.
13. DARGAHI A., SHOKOOHI R., ASGARI G., ANSARI A., NEMATOLLAHI D., SAMARGHANDI M.R. Moving-bed biofilm reactor combined with three-dimensional electrochemical pretreatment (MBBR-3DE) for 2,4-D herbicide treatment: application for real wastewater, improvement of biodegradability. RSC Advances, **11**, 9608, **2021**.
14. ZAHMATKESH Z., BURIAN S.J., KARAMOUZ M., TAVAKOL-DAVANI H., GOHARIAN E. Low-Impact development practices to mitigate climate change effects on urban stormwater runoff: case study of New York city. Journal of Irrigation & Drainage Engineering, **141** (1), 04014043, **2015**.
15. JOKAR D., KHAKZAND M., FAIZI M. The application of low impact development approaches toward achieving circularity in the water sector: a case study from Soltan Abad, shiraz, Iran. Journal of Cleaner Production, **320**, 128712, **2021**.
16. SHOKOOHI R., JAFARI A.J., DARGAHI A., TORKSHAVAND Z. Study of the efficiency of bio-filter and activated sludge (BF/AS) combined process in phenol removal from aqueous solution: determination of removing model according to response surface methodology (RSM). Desalination & Water Treatment, **77** (5), 256, **2017**.
17. MENG Y.Y., WANG H.X., ZHANG S.H., CHEN J.G. Suitability evaluation of plants in bioretention stormwater management measure. China Water & Wastewater, **31** (23), 142, **2015** [In Chinese].

18. YANG F.K., FU D.F., LIU S., ZEVENBERGEN C., SINGH R.P. Hydrologic and pollutant removal performance of media layers in bioretention. Water, **12** (3), 921, **2020**.

19. SHOKOOHI R., MOVAHEDIAN H., DARGAHI A., JAFARI A.J., PARVARESH A. Survey on efficiency of BF/AS integrated biological system in phenol removal of wastewater. Desalination and water treatment, **82** (7), 315, **2017**.

20. MINISTRY OF HOUSING AND URBAN-RURAL CONSTRUCTION OF THE PEOPLE'S REPUBLIC OF CHINA. Technical guideline for sponge city construction: construction of rainwater system with low impact development (Trial). Beijing: Ministry of Housing and Construction Rural Development, **2014**.

21. MACEDO M., LAGO C., MENDIONDO E.M. Stormwater volume reduction and water quality improvement by bioretention potentials and challenges for water security in a subtropical catchment. Archives of Pharmacal Research, **647**, 923, **2019**.

22. CHOWDHURY R., KSIKSI T., MOHAMED M.M.A., ABAYA J. Performance of vegetative bioretention system for greywater reuse in the arid climates. 8th International Conference on Environmental Science and Technology, Houston, United States of America, **2016**.

23. SUN Y.W., WEI X.M., POMEROY C.A. Global analysis of sensitivity of bioretention cell design elements to hydrologic performance. Water Science and Engineering, **4** (3), 12, **2011**.

24. LIU J., SAMPLE D.J., BELL C., GUAN Y.T. Review and research needs of bioretention used for the treatment of urban stormwater. Water, **6** (4), 1069, **2014**.

25. FASSMAN E., STOKES K. Media moisture content to determine evapotranspiration from swales and bioretention Cells. World Environmental and Water Resources Congress 2011, **2011**.

26. TANG S.C., LUO W., JIA Z.H., LI S., WU Y., ZHOU M. Effects of filler and rainfall characteristics on runoff reduction of rain garden and achieving the goal of sponge city construction, **30** (1), 73, **2016** [In Chinese].

27. WINSTON R.J., DORSEY J.D., HUNT W.F. Quantifying volume reduction and peak flow mitigation for three bioretention cells in clay soils in northeast Ohio. Science of the Total Environment, **553**, 83, **2016**.

28. PAN G.Y., XIA J., ZHANG X., WANG H.P., LIU E.M. Research on simulation test of hydrological effect of bioretention units. Water Resources and power, **30** (5), 13, **2012** [In Chinese].

29. GULBAZ S., KAZEZYILMAZ-ALHAN C.M. Experimental investigation on hydrologic performance of LID with rainfall-watershed-bioretention system. Journal of Hydrologic Engineering, **22** (1), D4016003, **2016**.

30. DEBUSK K.M., HUNT W.F., LINE D.E. Bioretention outflow: does it mimic nonurban watershed shallow interflow? Journal of Hydrologic Engineering, **16** (3), 274, **2010**.

31. GUO C., LI J.K., LI H.E., ZHANG B., MA M.H., ZHAO R.S. Impacts of stormwater concentrated infiltration in rainwater gardens on groundwater level and quality. Journal of Hydroelectric Engineering, **36** (12), 49, **2017** [In Chinese].

32. PAN J.K., LIU J.W., HU G.P., SU J.M., QIN G.Y. Long term hydrological effects of bioretention on expressway service area. Polish Journal of Environmental Studies, **31** (2), 1271, **2022**.

33. GAO J.P., PAN J.K., HU N., XIE C.Z. Hydrologic performance of bioretention in an expressway service area. Water Science & Technology, **77** (7), 1829, **2018**.

34. LI H.E., JIA B.K., CHENG B., GUO C., LI J.K. Research progress on the effect of concentrated runoff infiltration on soil and groundwater in sponge city. Advances in Water science, **30** (4), 589, **2019** [In Chinese].

35. LIANG H.H., LI X.L., ZHANG X., MA Y., JI G.Q., HU Z.P., LU Y.N. Optimization analysis of rainwater infiltration in bioretention zone near municipal roads. China Water & Wastewater, **36** (15), 107, **2020** [In Chinese].

36. WANG Q.Y., LI X.L., ZHANG X., WANG S.Q. Risk analysis of leakage location of bioretention zone in municipal roads. Science Technology and Engineering, **19** (27), 321, **2019**.

37. MAO X.Y., HUANG L.P. Design of municipal roads in mountainous city using low impact development technology based on sponge city concept. China Water & Wastewater, **32** (10), 81, **2016** [In Chinese].

38. BOANCA P.L., DUMITRAS A., LUCA L., BORS-OPRISA S. Analysing bioretention hydraulics and runoff retention through numerical modelling using RECARGA: a case study in a Romanian urban area. Polish Journal of Environmental Studies, **27** (5), 1965, **2018**.

39. MENG Y.Y., WANG H.X., CHEN J.G., ZHANG S.H. Modelling hydrology of a single bioretention system with HYDRUS-1D. The scientific world journal, 10.1155/2014/521047, **2014**.

40. FRIAS R.A., MANIQUIZ-REDILLAS M. Modelling the applicability of Low Impact Development (LID) technologies in a university campus in the Philippines using Storm Water Management Model (SWMM). IOP Conference Series: Materials Science and Engineering, **1153**, 012009, **2021**.

41. GAO J., WANG R.S., HUANG J.L., LIU M. Application of BMP to urban runoff control using SUSTAIN model: case study in an industrial area. Ecological Modelling, **318**, 177, **2015**.

42. JIAO Y.H., JIANG Z.Q. Study of the Effects on evapotranspiration to long-term stability of slope. Site Investigation Science and Technology, **5**, 3, **2009** [In Chinese].

43. GAO J.P., PAN J.K., XIE Y.C. Effects of bioretention structural layer parameters on detention and retention for road runoff. Advances in Water Science, **28** (5), 702, **2017** [In Chinese].

44. HE Z.X., DAVIS A.P. Process modeling of storm-water flow in a bioretention cell. Journal of Irrigation and Drainage Engineering, **137** (3), 121, **2011**.

45. GENUCHTEN M.T.V. A closed-form equation for predicting the hydraulic conductivity of unsaturated soils. Soil Science Society of America Journal, **44** (5), 892, **1980**.

46. LI Y., BUCHBERGER S.G., SANSALONE J.J. Variably saturated flow in storm-water partial exfiltration trench. Journal of Environmental Engineering, **125** (6), 556, **1999**.